Origins of Growth Stresses in Amorphous Semiconductor Thin Films

J. A. Floro, P. G. Kotula, and S. C. Seel
Sandia National Laboratories, Albuquerque, New Mexico 87185-1415, USA

D. J. Srolovitz
Princeton Materials Institute and Department of Mechanical and Aerospace Engineering, Princeton University, Princeton, New Jersey 08544-5263, USA
(Received 13 March 2003; published 28 August 2003)

Stress evolution during deposition of amorphous Si and Ge thin films is remarkably similar to that observed for polycrystalline films. Amorphous semiconductors were used as model materials to study the origins of deposition stresses in continuous films, where suppression of both strain relaxation and epitaxial strain inheritance provides considerable simplification. Our data show that bulk compression is established by surface stress, while a subsequent return to tensile stress arises from elastic coalescence processes occurring on the kinetically roughened surface.

DOI: 10.1103/PhysRevLett.91.096101 PACS numbers: 68.55.–a, 68.35.Gy, 68.35.–p

Real-time measurements of stress evolution during thin film deposition provide a surprisingly insightful window into dynamic processes occurring during Volmer-Weber (V-W) film growth [1,2]. The V-W mode, which occurs for film growth on dissimilar substrates, proceeds via nucleation and growth of discrete islands, coalescence, and (possibly) grain growth and surface evolution of the continuous polycrystalline film. Quantitative theoretical understanding of stress evolution during V-W growth has been limited by the complex structural evolution and because multiple stress generation and relaxation mechanisms can occur simultaneously. Furthermore, for polycrystalline films it is difficult to determine whether an observed stress state arises from a stress generation mechanism acting instantaneously, or whether the stress state is "inherited" via grain-by-grain epitaxial growth on a strained lattice established previously. In this Letter, we examine real-time stress evolution during deposition of amorphous Si (*a*:Si) and Ge (*a*:Ge) thin films. Simplifications associated with the use of amorphous films include (i) isotropy of elastic properties and interfacial energies, (ii) quenching of stress relaxation due to the low mobility growth conditions, and (iii) no epitaxial strain inheritance, implying that stresses are being produced "instantaneously," i.e., at the moment of observation. This study, which extends earlier work by Mayr and Samwer on amorphous metal alloys [3], provides the most definitive demonstration to date on the importance of surface stress in establishing bulk compression in continuous films, and on the importance of late-stage coalescence processes in establishing tensile stress in roughened but continuous films.

Films were grown by electron beam evaporation in ultrahigh vacuum [1,4]. Substrates were 100 μm thick Si (001) with native oxide, chemically cleaned then degassed *in vacuo* at 700 °C. Substrate curvature measurements were performed *in situ* using a multibeam optical stress sensor [1,4].

Figure 1 shows the "stress-thickness" product, proportional to substrate curvature, as a function of thickness for *a*:Ge deposited at 25 °C. The features of this curve are generically similar to those measured for many other V-W growth systems [1–3,5,6]. The initial tensile stress results from "zipping" processes occurring when discrete

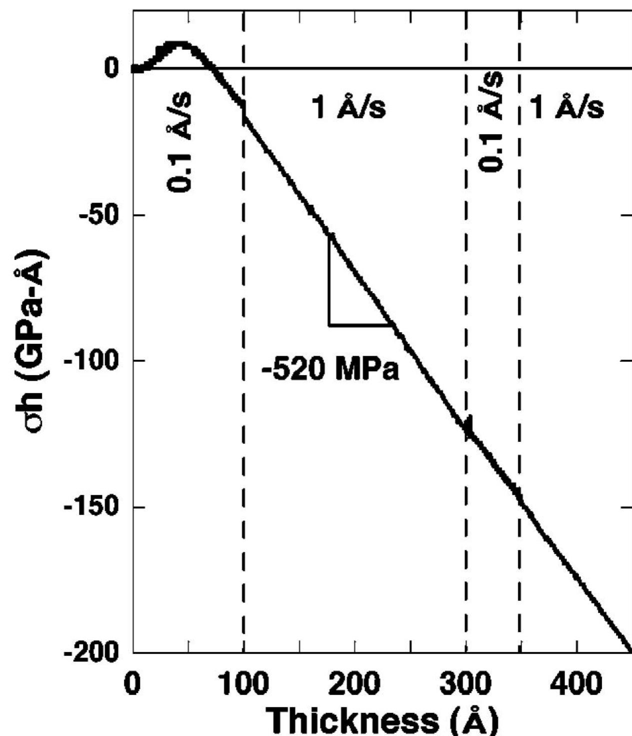

FIG. 1. Real-time substrate curvature evolution (plotted as the stress-thickness) during deposition of *a*:Ge at room temperature. Negative values represent compressive mean stress, while negative slopes represent compressive incremental stress. Within the steady-state compressive region, there is no change in the slope when deposition rate is varied by an order of magnitude.

 0031-9007/03/91(9)/096101(4)$20.00 © 2003 The American Physical Society

a:Ge islands on SiO_2 coalesce, deforming into contact to reduce surface energy at the expense of stored elastic energy [7–10]. After the film becomes continuous the incremental stress, represented by the slope of the curve, becomes compressive. Within this regime, the deposition rate was varied by an order of magnitude, with no effect on the steady-state compression (about -520 MPa). No time-dependent behavior was observed during growth interrupts, demonstrating complete quenching of stress relaxation.

Figure 2 shows the stress-thickness for *a*:Si films grown at 0.5 Å/s and at 25 °C, 90 °C, and 150 °C [11]. While the initial behavior is the same as for *a*:Ge, a new feature is the return to tensile stress, which occurs at larger thickness for higher deposition temperature. At 90 °C and 150 °C, the compressive stress regime exhibits similar stress magnitudes. Growth interrupts again demonstrate that no stress relaxation is occurring in this temperature range.

To compare the coupled evolution of stress and microstructure, the following sample was grown at 90 °C: 1225 Å *a*:Si containing two buried pairs of *a*:Ge marker layers. Each marker pair was 2.5 Å of *a*:Ge separated by 35 Å. This was followed by an 800 Å *a*:Ge layer with two pairs of *a*:Si markers arranged in similar fashion as in the underlying layer. The markers provide a snapshot of the time-dependent surface morphology using annular dark-field scanning transmission electron microscopy (ADF-STEM) [12] as shown in the cross section of Fig. 3(a), with the corresponding stress evolution shown in Fig. 3(b). The *a*:Si layer evolves from tension (coalescence) to compression (continuity) and back to tension as described above. The subsequent *a*:Ge layer does not replicate the tension in the *a*:Si, but grows in compression similar to growth of *a*:Ge directly on the SiO_2 substrate (see Fig. 1). A significant feature of the *a*:Si image in Fig. 3(a) is the presence of a dense array of irregular, bands parallel to the growth direction. A much smaller density of these features is observed in the *a*:Ge layer. Figure 4(a) shows a high-resolution TEM image of the *a*:Si layer that confirms that these features are nanovoid tracks similar to those observed previously in ultrahigh vacuum vapor-deposited *a*:Si [13] and in low-temperature Si homoepitaxy [14]. The depth at which these void tracks initiate corresponds exactly to where the compressive stress reverses into tension.

Figures 4(b) and 4(c) show enlargements of the marker layer regions. The marker morphology shows that thickness-dependent roughening of the growth fronts clearly occurred, with *a*:Si exhibiting significantly higher spatial frequencies and apparent aspect ratios than *a*:Ge [15]. Careful examination reveals that void tracks align with cusps in the dynamic growth surface. Features on the Ge free surface also correlate well with features in the buried markers, although effects of subsequent air exposure on the Ge surface roughness cannot be entirely ruled out.

While a variety of mechanisms have been proposed for compressive stress generation [2,16–20], the lack of both a rate and temperature dependence to the magnitude of

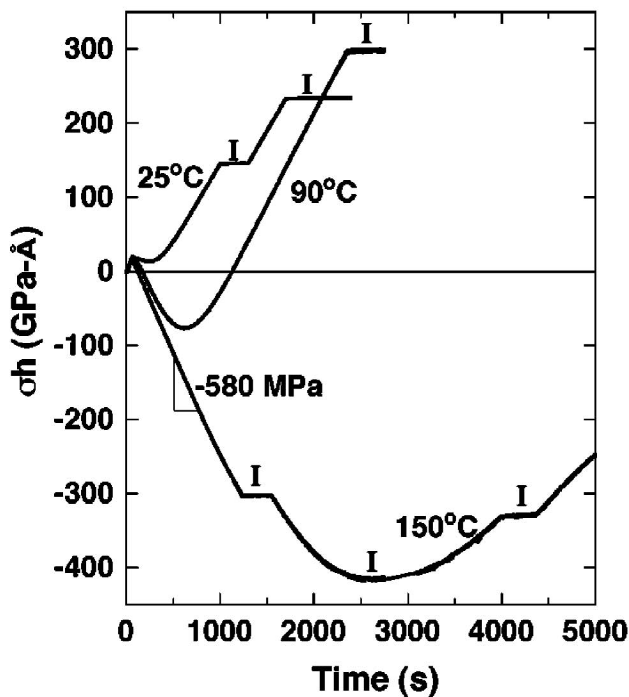

FIG. 2. Real-time substrate curvature evolution vs time during deposition of *a*:Si at various temperatures, plotted vs time to highlight growth interrupts (“I”). After a compressive regime, all films return to tension.

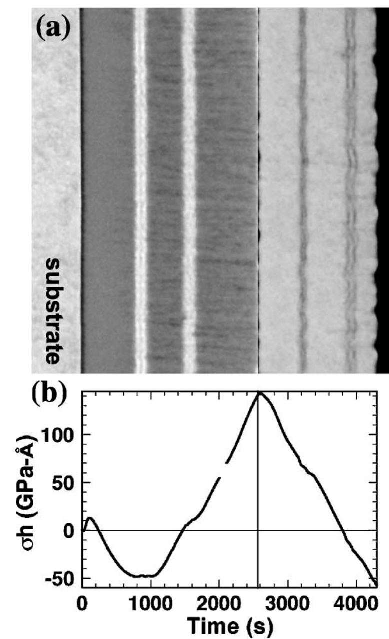

FIG. 3. (a) Composite ADF-STEM image using optimized contrast conditions for each layer, showing markers and void tracks. (b) Real-time substrate curvature evolution for the bilayer film structure containing thin marker layers. Arrows highlight the effect of the marker layers on the curvature.

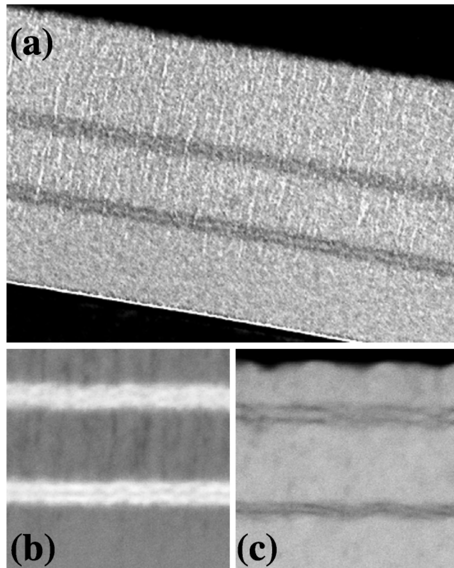

FIG. 4. (a) High resolution bright field XTEM image of nanovoid tracks in *a*:Si. Enlarged views of the marker layer morphology from ADF-STEM in (b) *a*:Si and (c) *a*:Ge.

the compression is consistent only with stress generation due to surface stress [19,20]. In crystalline materials, surface stress (here assumed to be tensile) imposes a reduced lattice parameter upon a thin film relative to bulk material. The reduced lattice parameter is locked-in during the percolation phase of growth (thickness h_{perc}), and subsequent epitaxial growth on this layer occurs in a state of increasing compressive stress that saturates at a limiting value of $-(F+G)/h_{\mathrm{perc}}$, where F (G) is the surface (interface) stress.

For an amorphous film, constant compression implies continuous generation of stress due to the *instantaneous* action of surface stress. Atoms adding to the growth surface of an amorphous solid (where lattice-imposed constraints on adatom incorporation are reduced compared to crystals) can pack closer to increase their local electron density, thereby creating an excess atomic density in the near-surface layers relative to the "ideal" density of fully coordinated bulk material. When the surface layer is buried by further deposition and becomes bulk coordinated, expansion of the layer is suppressed and a compressive stress is thereby established. An excess areal density of 1% will produce the observed stress of -500 MPa. Gill *et al.* recently discussed this mechanism in terms of a "local transformation strain" [21] that is related to the surface stress as $\sigma = -\mathrm{F}/h_{\mathrm{surf}}$, where h_{surf} is the effective thickness of the surface layer. Taking $F = 1\ \mathrm{J/m^2}$, and $h_{\mathrm{surf}} = 5$ Å, $\sigma = -2$ GPa, which is an upper bound estimate on the stress.

The subsequent change from compressive stress back into tension for *a*:Si films directly correlates with the formation of nanovoid tracks that develop when the surface becomes sufficiently rough. Molecular dynamics growth simulations of Smith and Srolovitz show that low adatom mobility promotes formation of deep cusplike features on the growth surface [22]. Cusps can become incipient voids with further deposition, as adatoms aggregating near the upper surface of the cusp shadow the lower surface from the flux. When aggregates on opposing sides of a cusp approach to within an atomic diameter of one another, they often snap together across the gap, sealing off the cusp to form a fully enclosed void and creating a residual strain field, which is a related process to the island zipping mechanisms used to explain tensile stress generation in the early stages of film growth [7–10]. While it would seem natural to invoke the void sealing mechanism to explain the tensile stress in *a*:Si, straightforward calculations indicate that the void concentration would need to be 20 times higher than observed to account for the measured stress levels. However, void formation does indicate that extreme surface roughness developed, and that related zipping mechanisms then occurred [23]. Mayr and Samwer [3] showed that mounds develop on the surface of amorphous metal alloys and suggested that zipping occurs at the root of the mounds. Mound formation is apparent in our TEM cross-section images, such as those shown in Fig. 4, where both the free Ge surface and the marker layers show significant roughening. Figure 5 shows a sketch of a close-packed array of hemispherical mounds zipping from their contact points. Voids would most likely be created at the triple junctions between the mounds in the manner described in Ref. [22].

Freund and Chason previously modeled zipping of a coplanar array of hemispheres in detail and obtained an expression for the mean stress, $\langle\sigma\rangle = 6\gamma/R$ [9,24], where γ is the reduction in surface energy that drives zipping. While the mound radius is the primary variable

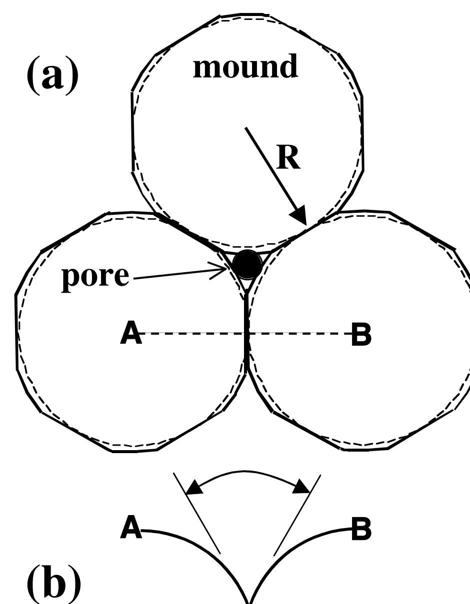

FIG. 5. (a) Plan-view illustration of zipping of hemispherical mounds and pore formation: dashed lines, prior to zipping; solid lines, after zipping. (b) Cross section view from A to B prior to zipping to define the dihedral angle.

controlling the magnitude of the zipping stress, it has recently been shown that the stress also exhibits a strong inverse dependence on the dihedral angle, defined in Fig. 5(b) [25]. Based on the measured void track density, and assuming the hexagonal arrangement of void tracks shown in Fig. 5, we estimate the in-plane mound radius $R = 114 \pm 35$ Å. Using this, we arrive at $\langle\sigma\rangle = 0.53 \pm 0.13$ GPa, in good agreement with the observed stress, 0.55 GPa, implying that the dihedral angle is near 0°. The lack of epitaxial strain inheritance implies that roughening and zipping must occur continuously in the late-stage tensile regime.

The large temperature sensitivity to the onset of tensile stress in *a*:Si is consistent with thermally activated surface diffusion, which should retard kinetic roughening at elevated temperatures. In agreement with this, roughening transitions under low mobility *a*:Si growth conditions have been observed previously using real-time spectroscopic ellipsometry; roughening was suppressed when adspecies mobility was increased [26]. We found no tensile zipping stress in *a*:Ge, suggesting that higher surface self-diffusivity results in a larger lateral length scale (R) to the roughness, and a larger contact angle at the cusp between mounds (reduced aspect ratio compared to *a*:Si).

In summary, amorphous semiconductor films were used as model materials in which to study the origins of deposition stresses in thin films. Suppression of epitaxial strain inheritance permits unambiguous deconvolution of stress generation mechanisms as the film thickens. Compressive stress was both rate and temperature independent, indicating that compression resulted from incorporation of excess atomic density due to surface stress. A subsequent return to tensile stress in *a*:Si correlated with the formation of high aspect ratio surface mounds and internal nanovoid tracks, strongly implying that zipping occurred in the rough but continuous film. The stress generation mechanisms discussed here are quite generic in their applicability to thin films, and will also be important in understanding stresses in free-standing and/or sintered nanoparticles.

The authors acknowledge invaluable discussions with Bob Cammarata, Bill Nix, Mike Aziz, Sean Hearne, and Hal Kahn. Our thanks to Jess Floro and Josh Miera for experimental help. This work was supported by the Division of Materials Science and Engineering, Office of Science, U.S. Department of Energy. Sandia is a multiprogram laboratory operated by Sandia Corporation, a Lockheed Martin Company, for the United States Department of Energy under Contract No. DE-AC04-94AL85000.

[1] J. A. Floro, S. J. Hearne, J. A. Hunter, P. Kotula, E. Chason, S. C. Seel, and C. V. Thompson, J. Appl. Phys. **89**, 4886 (2001).
[2] Jerrold A. Floro, Eric Chason, Robert C. Cammarata, and David J. Srolovitz, MRS Bull. **28**, 19 (2002).
[3] S. G. Mayr and K. Samwer, Phys. Rev. Lett. **87**, 6105 (2001).
[4] J. A. Floro, E. Chason, L. B. Freund, R. D. Twesten, and R. Q. Hwang, Phys. Rev. B **59**, 1990 (1999).
[5] R. Koch, J. Phys. Condens. Matter **6**, 9519 (1994).
[6] Alison Shull and Frans Spaepen, J. Appl. Phys. **80**, 6243 (1996).
[7] R. W. Hoffman, Thin Solid Films **34**, 185 (1976).
[8] W. B. Nix and B. M. Clemens, J. Mater. Res. **14**, 3467 (1999).
[9] L. B. Freund and E. Chason, J. Appl. Phys. **89**, 4866 (2001).
[10] S. C. Seel, C. V. Thompson, S. J. Hearne, and J. A. Floro, J. Appl. Phys. **88**, 7079 (2000).
[11] These measurements are based on separate calibrations of temperature vs heater current obtained using a thermocouple bonded to the Si wafer.
[12] D. E. Jesson, S. J. Pennycook, J.-M. Baribeau, and D. C. Houghton, Phys. Rev. Lett. **71**, 1744 (1993).
[13] M. J. J. Theunissen, J. M. L. van Rooij-Mulder, C. W. T. Bulle-Lieuwma, D. E. W. Vandenoutdt, D. J. Gravesteijn, and G. FA. van de Walle, J. Cryst. Growth **118**, 125 (1992).
[14] D. D. Perovic, G. C. Weatherly, P. J. Simpson, P. J. Schultz, T. E. Jackman, G. C. Aers, J. P. Noel, and D. C. Houghton, Phys. Rev. B **43**, 14257 (1991).
[15] The spatial period of the roughness is smaller than the thickness of the cross section.
[16] E. Chason, B. W. Sheldon, L. B. Freund, J. A. Floro, and S J. Hearne, Phys. Rev. Lett. **88**, 156103 (2002).
[17] F. Spaepen, Acta Mater. **48**, 31 (2000).
[18] C. Friesen and C. V. Thompson, Phys. Rev. Lett. **89**, 126103 (2002).
[19] R. C. Cammarata, Prog. Surf. Sci. **46**, 1 (1994).
[20] R. C. Cammarata, T. M. Trimble, and D. J. Srolovitz, J. Mater. Res. **15**, 2468 (2000).
[21] S. P. A. Gill, H. Gao, V. Ramaswamy, and W. D. Nix, J. Appl. Mech. **69**, 425 (2002).
[22] Richard W. Smith and David J. Srolovitz, J. Appl. Phys. **79**, 1448 (1996).
[23] B. W. Sheldon, K. H. A. Lau, and A. Rajamani, J. Appl. Phys. **90**, 5097 (2001).
[24] Freund and Chason's result [9] is actually $\langle\sigma\rangle = 4\gamma/R$ for a fourfold symmetric array of islands, which we have modified for the sixfold symmetric mound geometry used here, and in [3].
[25] S. C. Seel and C. V. Thompson, J. Appl. Phys. 93, 9038 (2003).
[26] R. W. Collins and A. S. Ferlauto, Curr. Opin. Solid State Matter Sci. **6**, 425 (2002).